arXiv:hep-ex/0312048v1 17 Dec 2003

Search for QCD-instanton induced events in deep inelastic ep scattering at HERA

ZEUS Collaboration

Abstract

A search for QCD-instanton-induced events in deep inelastic ep scattering has been performed with the ZEUS detector at the HERA collider, using data corresponding to an integrated luminosity of $38\,\mathrm{pb}^{-1}$. A kinematic range defined by cuts on the photon virtuality, $Q^2 > 120\,\mathrm{GeV}^2$, and on the Bjorken scaling variable, $x > 10^{-3}$, has been investigated. The QCD-instanton induced events were modelled by the Monte Carlo generator QCDINS. A background-independent, conservative 95% confidence level upper limit for the instanton cross section of $26\,\mathrm{pb}$ is obtained, to be compared with the theoretically expected value of $8.9\,\mathrm{pb}$.

The ZEUS Collaboration

S. Chekanov, M. Derrick, D. Krakauer, J.H. Loizides[1], S. Magill, S. Miglioranzi[1], B. Musgrave, J. Repond, R. Yoshida
Argonne National Laboratory, Argonne, Illinois 60439-4815, USA [n]

M.C.K. Mattingly
Andrews University, Berrien Springs, Michigan 49104-0380, USA

P. Antonioli, G. Bari, M. Basile, L. Bellagamba, D. Boscherini, A. Bruni, G. Bruni, G. Cara Romeo, L. Cifarelli, F. Cindolo, A. Contin, M. Corradi, S. De Pasquale, P. Giusti, G. Iacobucci, A. Margotti, A. Montanari, R. Nania, F. Palmonari, A. Pesci, G. Sartorelli, A. Zichichi
University and INFN Bologna, Bologna, Italy [e]

G. Aghuzumtsyan, D. Bartsch, I. Brock, S. Goers, H. Hartmann, E. Hilger, P. Irrgang, H.-P. Jakob, O. Kind, U. Meyer, E. Paul[2], J. Rautenberg, R. Renner, A. Stifutkin, J. Tandler, K.C. Voss, M. Wang, A. Weber[3]
Physikalisches Institut der Universität Bonn, Bonn, Germany [b]

D.S. Bailey[4], N.H. Brook, J.E. Cole, G.P. Heath, T. Namsoo, S. Robins, M. Wing
H.H. Wills Physics Laboratory, University of Bristol, Bristol, United Kingdom [m]

M. Capua, A. Mastroberardino, M. Schioppa, G. Susinno
Calabria University, Physics Department and INFN, Cosenza, Italy [e]

J.Y. Kim, Y.K. Kim, J.H. Lee, I.T. Lim, M.Y. Pac[5]
Chonnam National University, Kwangju, Korea [g]

A. Caldwell[6], M. Helbich, X. Liu, B. Mellado, Y. Ning, S. Paganis, Z. Ren, W.B. Schmidke, F. Sciulli
Nevis Laboratories, Columbia University, Irvington on Hudson, New York 10027 [o]

J. Chwastowski, A. Eskreys, J. Figiel, A. Galas, K. Olkiewicz, P. Stopa, L. Zawiejski
Institute of Nuclear Physics, Cracow, Poland [i]

L. Adamczyk, T. Bołd, I. Grabowska-Bołd[7], D. Kisielewska, A.M. Kowal, M. Kowal, T. Kowalski, M. Przybycień, L. Suszycki, D. Szuba, J. Szuba[8]
Faculty of Physics and Nuclear Techniques, AGH-University of Science and Technology, Cracow, Poland [p]

A. Kotański[9], W. Słomiński
Department of Physics, Jagellonian University, Cracow, Poland

V. Adler, U. Behrens, I. Bloch, K. Borras, V. Chiochia, D. Dannheim, G. Drews, J. Fourletova,
U. Fricke, A. Geiser, P. Göttlicher[10], O. Gutsche, T. Haas, W. Hain, S. Hillert[11], B. Kahle,
U. Kötz, H. Kowalski[12], G. Kramberger, H. Labes, D. Lelas, H. Lim, B. Löhr, R. Mankel,
I.-A. Melzer-Pellmann, C.N. Nguyen, D. Notz, A.E. Nuncio-Quiroz, A. Polini, A. Raval,
L. Rurua, U. Schneekloth, U. Stoesslein, G. Wolf, C. Youngman, W. Zeuner
Deutsches Elektronen-Synchrotron DESY, Hamburg, Germany

S. Schlenstedt
DESY Zeuthen, Zeuthen, Germany

G. Barbagli, E. Gallo, C. Genta, P. G. Pelfer
University and INFN, Florence, Italy [e]

A. Bamberger, A. Benen, F. Karstens, D. Dobur, N.N. Vlasov
Fakultät für Physik der Universität Freiburg i.Br., Freiburg i.Br., Germany [b]

M. Bell, P.J. Bussey, A.T. Doyle, J. Ferrando, J. Hamilton, S. Hanlon, D.H. Saxon,
I.O. Skillicorn
Department of Physics and Astronomy, University of Glasgow, Glasgow, United Kingdom [m]

I. Gialas
Department of Engineering in Management and Finance, Univ. of Aegean, Greece

B. Bodmann, T. Carli, U. Holm, K. Klimek, N. Krumnack, E. Lohrmann, M. Milite,
H. Salehi, P. Schleper, S. Stonjek[11], K. Wick, A. Ziegler, Ar. Ziegler
Hamburg University, Institute of Exp. Physics, Hamburg, Germany [b]

C. Collins-Tooth, C. Foudas, R. Gonçalo[13], K.R. Long, A.D. Tapper
Imperial College London, High Energy Nuclear Physics Group, London, United Kingdom [m]

P. Cloth, D. Filges
Forschungszentrum Jülich, Institut für Kernphysik, Jülich, Germany

M. Kataoka[14], K. Nagano, K. Tokushuku[15], S. Yamada, Y. Yamazaki
Institute of Particle and Nuclear Studies, KEK, Tsukuba, Japan [f]

A.N. Barakbaev, E.G. Boos, N.S. Pokrovskiy, B.O. Zhautykov
Institute of Physics and Technology of Ministry of Education and Science of Kazakhstan, Almaty, Kazakhstan

D. Son
Kyungpook National University, Center for High Energy Physics, Daegu, South Korea [g]

K. Piotrzkowski

Institut de Physique Nucléaire, Université Catholique de Louvain, Louvain-la-Neuve, Belgium

F. Barreiro, C. Glasman[16], O. González, L. Labarga, J. del Peso, E. Tassi, J. Terrón, M. Vázquez, M. Zambrana

Departamento de Física Teórica, Universidad Autónoma de Madrid, Madrid, Spain [l]

M. Barbi, F. Corriveau, S. Gliga, J. Lainesse, S. Padhi, D.G. Stairs, R. Walsh

Department of Physics, McGill University, Montréal, Québec, Canada H3A 2T8 [a]

T. Tsurugai

Meiji Gakuin University, Faculty of General Education, Yokohama, Japan [f]

A. Antonov, P. Danilov, B.A. Dolgoshein, D. Gladkov, V. Sosnovtsev, S. Suchkov

Moscow Engineering Physics Institute, Moscow, Russia [j]

R.K. Dementiev, P.F. Ermolov, Yu.A. Golubkov[17], I.I. Katkov, L.A. Khein, I.A. Korzhavina, V.A. Kuzmin, B.B. Levchenko[18], O.Yu. Lukina, A.S. Proskuryakov, L.M. Shcheglova, S.A. Zotkin

Moscow State University, Institute of Nuclear Physics, Moscow, Russia [k]

N. Coppola, S. Grijpink, E. Koffeman, P. Kooijman, E. Maddox, A. Pellegrino, S. Schagen, H. Tiecke, J.J. Velthuis, L. Wiggers, E. de Wolf

NIKHEF and University of Amsterdam, Amsterdam, Netherlands [h]

N. Brümmer, B. Bylsma, L.S. Durkin, T.Y. Ling

Physics Department, Ohio State University, Columbus, Ohio 43210 [n]

A.M. Cooper-Sarkar, A. Cottrell, R.C.E. Devenish, B. Foster, G. Grzelak, C. Gwenlan[19], S. Patel, P.B. Straub, R. Walczak

Department of Physics, University of Oxford, Oxford United Kingdom [m]

A. Bertolin, R. Brugnera, R. Carlin, F. Dal Corso, S. Dusini, A. Garfagnini, S. Limentani, A. Longhin, A. Parenti, M. Posocco, L. Stanco, M. Turcato

Dipartimento di Fisica dell' Università and INFN, Padova, Italy [e]

E.A. Heaphy, F. Metlica, B.Y. Oh, J.J. Whitmore[20]

Department of Physics, Pennsylvania State University, University Park, Pennsylvania 16802 [o]

Y. Iga

Polytechnic University, Sagamihara, Japan [f]

G. D'Agostini, G. Marini, A. Nigro

Dipartimento di Fisica, Università 'La Sapienza' and INFN, Rome, Italy [e]

C. Cormack[21], J.C. Hart, N.A. McCubbin
Rutherford Appleton Laboratory, Chilton, Didcot, Oxon, United Kingdom [m]

C. Heusch
University of California, Santa Cruz, California 95064, USA [n]

I.H. Park
Department of Physics, Ewha Womans University, Seoul, Korea

N. Pavel
Fachbereich Physik der Universität-Gesamthochschule Siegen, Germany

H. Abramowicz, A. Gabareen, S. Kananov, A. Kreisel, A. Levy
Raymond and Beverly Sackler Faculty of Exact Sciences, School of Physics, Tel-Aviv University, Tel-Aviv, Israel [d]

M. Kuze
Department of Physics, Tokyo Institute of Technology, Tokyo, Japan [f]

T. Fusayasu, S. Kagawa, T. Kohno, T. Tawara, T. Yamashita
Department of Physics, University of Tokyo, Tokyo, Japan [f]

R. Hamatsu, T. Hirose[2], M. Inuzuka, H. Kaji, S. Kitamura[22], K. Matsuzawa
Tokyo Metropolitan University, Department of Physics, Tokyo, Japan [f]

M.I. Ferrero, V. Monaco, R. Sacchi, A. Solano
Università di Torino and INFN, Torino, Italy [e]

M. Arneodo, M. Ruspa
Università del Piemonte Orientale, Novara, and INFN, Torino, Italy [e]

T. Koop, G.M. Levman, J.F. Martin, A. Mirea
Department of Physics, University of Toronto, Toronto, Ontario, Canada M5S 1A7 [a]

J.M. Butterworth[23], R. Hall-Wilton, T.W. Jones, M.S. Lightwood, M.R. Sutton[4], C. Targett-Adams
Physics and Astronomy Department, University College London, London, United Kingdom [m]

J. Ciborowski[24], R. Ciesielski[25], P. Łużniak[26], R.J. Nowak, J.M. Pawlak, J. Sztuk[27], T. Tymieniecka[28], A. Ukleja[28], J. Ukleja[29], A.F. Żarnecki
Warsaw University, Institute of Experimental Physics, Warsaw, Poland [q]

M. Adamus, P. Plucinski
Institute for Nuclear Studies, Warsaw, Poland [q]

Y. Eisenberg, L.K. Gladilin[30], D. Hochman, U. Karshon M. Riveline
Department of Particle Physics, Weizmann Institute, Rehovot, Israel [c]

D. Kçira, S. Lammers, L. Li, D.D. Reeder, M. Rosin, A.A. Savin, W.H. Smith
Department of Physics, University of Wisconsin, Madison, Wisconsin 53706, USA [n]

A. Deshpande, S. Dhawan
Department of Physics, Yale University, New Haven, Connecticut 06520-8121, USA [n]

S. Bhadra, C.D. Catterall, S. Fourletov, G. Hartner, S. Menary, M. Soares, J. Standage
Department of Physics, York University, Ontario, Canada M3J 1P3 [a]

1 Introduction

In the Standard Model, both the strong and the electroweak interactions are described by non-Abelian gauge theories. In such theories, the ground state has a rich topological structure, associated with non-perturbative fluctuations of the gauge fields [1], called instantons [2]. They can be interpreted as tunneling processes of the gauge fields between topologically distinct types of vacuum states.

Although the existence of instantons is required by the Standard Model, they have not been observed. While in electroweak interactions instantons are predicted to play a role only at centre-of-mass energies $\gg 10\,\text{TeV}$ [3, 4], QCD instanton effects are expected to become sizeable at much lower energies, where they are predicted to have short-distance implications [5,4,6,7]. In particular, they can induce characteristic events in deep inelastic scattering (DIS). The HERA ep collider offers a unique opportunity to discover instantons. Their discovery would constitute a confirmation of an essential non-perturbative Standard Model prediction, connected with the QCD vacuum. Results of such a search have recently been reported by the H1 collaboration [8].

Since instanton-induced events are predicted to contribute less than 1% to the cross section of the neutral current DIS sample used in this search, it is essential to find variables that efficiently discriminate between instanton and standard DIS events. Statistical discrimination methods have been employed to obtain event samples with a larger fraction of instanton events in a search for a possible signal.

2 Experimental setup

The data sample used in this search corresponds to an integrated luminosity of $38.3 \pm 0.6\,\text{pb}^{-1}$ collected with the ZEUS detector at the HERA collider. During the years 1996 and 1997, positrons of energy $E_e = 27.5\,\text{GeV}$ collided with protons of energy $E_p = 820\,\text{GeV}$. A detailed description of the ZEUS detector can be found elsewhere [9]. The main detector components used in the search presented here are the central tracking detector (CTD) [10], operating in a magnetic field of 1.43 T provided by a thin superconducting solenoid, and the uranium-scintillator calorimeter (CAL) [11].

Tracking information is provided by the CTD, in which the momenta of tracks in the polar-angle[1] region $15° < \theta < 164°$ are reconstructed. The CTD consists of 72 cylindrical

---

[1] The ZEUS coordinate system is a right-handed Cartesian system, with the Z axis pointing in the proton beam direction, referred to as the "forward direction", and the X axis pointing left towards the centre of HERA. The coordinate origin is at the nominal interaction point.

drift chamber layers, organised in nine superlayers. The relative transverse-momentum resolution for full-length tracks is $\sigma(p_T)/p_T = 0.0058 p_T \oplus 0.0065 \oplus 0.0014/p_T$, with p_T in GeV.

The CAL covers 99.7% of the total solid angle. It is divided into three parts with a corresponding division in θ, as viewed from the nominal interaction point: forward (FCAL, $2.6° < \theta < 36.7°$), barrel (BCAL, $36.7° < \theta < 129.1°$), and rear (RCAL, $129.1° < \theta < 176.2°$). Each of the CAL parts is subdivided into towers, which in turn are segmented longitudinally into one electromagnetic (EMC) and one (RCAL) or two (FCAL, BCAL) hadronic (HAC) sections. The smallest subdivision of the CAL is called a cell. Under test-beam conditions, the CAL single-particle relative energy resolution was $\sigma(E)/E = 0.18/\sqrt{E}$ for electrons and $\sigma(E)/E = 0.35/\sqrt{E}$ for hadrons, with E in GeV.

The luminosity was measured using the Bethe-Heitler reaction $ep \rightarrow e\gamma p$. The resulting small-angle energetic photons were measured by the luminosity monitor [12], a lead-scintillator calorimeter placed in the HERA tunnel at $Z = -107\,\text{m}$.

3 Characteristics of instanton-induced events

Ringwald and Schrempp [4, 6, 13, 7, 14, 15] have identified kinematic regions in DIS that allow a perturbative calculation of instanton-induced processes. These processes lead to a characteristic final state, which may allow instanton-induced events to be distinguished from standard DIS processes. Figure 1 shows a diagram of an instanton-induced event in an ep collision. The incoming lepton emits a photon, with four-vector q, which in turn transforms into a quark-antiquark pair. One of these quarks hadronises to form the current jet with four-vector q''. The other quark, with four-vector q', fuses with a gluon (four-vector g) from the proton in the presence of an instanton. The phenomenological characteristics of instanton-induced events can be summarised as follows [4]: in the hard subprocess exactly one $q\bar{q}$ pair of each of the n_f kinematically accessible quark flavours participates in the quark gluon fusion process, either as incoming or outgoing fermion line. This gives rise to a high-multiplicity final state. The produced particles are expected to be isotropically distributed in their centre-of-mass frame. In addition, the events have large transverse energy in the hadronic centre-of-mass frame.

Instanton-induced events in DIS were simulated using the Monte Carlo (MC) generator QCDINS 2.0 [14], which simulates the hard subprocess in the presence of an instanton. For the description of parton showers and hadronisation, HERWIG 5.9 [16] is used. The simulation of the hard subprocess is accomplished by applying instanton perturbation theory around the one-instanton solution. By comparing the results obtained from instanton perturbation theory to those from lattice simulations of QCD, the fiducial region

of the QCDINS MC program has been derived [7] in terms of the kinematic variables $Q'^2 = -q'^2 = -(q - q'')^2$, $x' = Q'^2/(2g \cdot q')$ and $Q^2 = -q^2$, describing the hard subprocess of instanton-induced events:

$$Q' \geq Q'_{\min} = 30.8 \cdot \Lambda_{\overline{\mathrm{MS}}}^{(n_f)} = \sqrt{113\,\mathrm{GeV}^2} \qquad ; \quad x' \geq x'_{\min} = 0.35,$$

where $\Lambda_{\overline{\mathrm{MS}}}^{(n_f)}$ is the QCD scale.

For QCDINS, cuts on the generated x' and Q'^2 variables were made at the values given above in order to restrict the sample to the region where the calculation is reliable. Non-planar contributions [6], which are not taken into account in the calculation, were suppressed by a cut on the photon virtuality, $Q^2 \geq Q^2_{\min} = Q'^2_{\min}$.

The generated events were passed through the GEANT 3.13 -based [17] ZEUS detector- and trigger-simulation programs. They were reconstructed and analysed using the same program chain as the data.

4   Simulation of standard DIS events

Standard DIS events were generated using the LEPTO 6.5 program [18] interfaced to HERACLES [19] via DJANGOH 1.1 [20]. The HERACLES program includes first-order electroweak radiative corrections. The CTEQ4 [21] proton parton distribution functions (PDF) were used. The QCD radiation was modelled with the colour-dipole model (CDM) [22] by using the ARIADNE 4.10 program [23]. Fragmentation into hadrons was performed using the Lund string model [24] as implemented in JETSET [25]. In order to improve the description of the sphericity distribution in the hadronic final state (see Section 6), the width of the transverse momentum distribution of primary hadrons (i.e. JETSET parameter PARJ(21)) was lowered to $0.28\,\mathrm{GeV}$. The diffractive contribution to the neutral current sample was taken into account by adding 12% of diffractive RAPGAP events. This percentage was determined from a fit of the distribution of the variable $\eta_{\max}$ [26], which is the pseudorapidity of the calorimeter energy deposit with the smallest polar angle and an energy above $400\,\mathrm{MeV}$. In what follows, the term DJANGOH always refers to the combination of DJANGOH and RAPGAP. For a cross-check of the results, the generator HERWIG 5.9 [16] has been used; this program also provides the description of parton showers and hadronisation for the QCDINS MC. In HERWIG, coherence effects in the final-state cascade are included by angular ordering of successive parton emissions, and a clustering model is used for hadronisation [27]. Electroweak radiative effects are not included in HERWIG. Detector resolution and selection efficiency were simulated as for the signal sample (see Section 3).

5 Event Selection and Reconstruction

5.1 Reconstruction of kinematic variables

Both track and calorimeter information were used for event reconstruction. Calorimeter cells were first grouped to form clusters which were then associated with tracks, where possible, to form energy-flow objects (EFOs) [28]. The hadronic final state of an event comprises all EFOs that do not stem from the scattered positron.

Positron identification was based on the pattern of energy deposits in the CAL [29]. The positron energy E_{DA} was calculated using the double angle (DA) method [30]. Tracking information was used to determine the positron polar angle, if the polar angle in the CAL was above 0.3 rad and if the track traversed more than three CTD superlayers. Otherwise these angles were determined from the CAL information.

The kinematic region investigated was defined by cuts on Q^2, and on the Bjorken scaling variables x and y. The variables Q^2 and x were reconstructed using the DA method, and y was reconstructed using the Jacquet-Blondel method [31].

In order to reconstruct the kinematic variable Q'^2 (see Fig. 1), EFOs were assigned to the current jet or to the instanton part of the hadronic final state. The current jet was identified by applying the k_T-cluster algorithm [32] in the longitudinally invariant mode [33] on all EFOs in the hadronic centre-of-mass frame (hcms). The photon direction was chosen as the negative Z direction. Monte Carlo studies showed, that in a region where the cross section for instanton related events is enhanced, and for high transverse jet momenta, the current quark has, on average, a smaller pseudorapidity than the partons assigned to the instanton. The current jet was therefore found as follows: a list of jets with a pseudorapidity $\eta_{\mathrm{jet}}^{\mathrm{hcms}}$ less than the transverse-momentum-weighted mean pseudorapidity of all EFOs in the hadronic final state was made ($\eta_{\mathrm{jet}}^{\mathrm{hcms}} < \sum_{\mathrm{EFOs}} \eta \cdot p_T / \sum_{\mathrm{EFOs}} p_T$). Here the jet pseudorapidity was calculated from the jet four-momentum, obtained by summing the four-momenta of all the EFOs assigned to the jet. Of the jets in the list, the one with the highest transverse momentum was chosen as the current jet.

The variable Q'^2_{DA} was calculated using the expression

$$Q'^2_{\mathrm{DA}} = Q^2_{\mathrm{DA}} + \frac{W^2_{\mathrm{DA}} - Q^2_{\mathrm{DA}}}{W_{\mathrm{DA}}} \cdot \sum_{i \in \mathrm{jet}} E_i - \frac{W^2_{\mathrm{DA}} + Q^2_{\mathrm{DA}}}{W_{\mathrm{DA}}} \cdot \sum_{i \in \mathrm{jet}} p_{Z,i} - M^2_{\mathrm{jet}} \ ,$$

with

$$W_{\mathrm{DA}} = \sqrt{Q^2_{\mathrm{DA}}(1 - x_{\mathrm{DA}})/x_{\mathrm{DA}} + m^2_p} \ ,$$

where M_{jet} is the current jet mass and m_p the proton mass. According to MC studies, Q'^2 is reconstructed with a relative accuracy of about 30%. However, the distribution of the reconstructed Q'^2 has a long tail in the direction of overestimation of the true value.

5.2 Selection of neutral current DIS events

A three-level trigger [9, 34] was used to select events online. A high-Q^2 neutral current DIS sample was selected requiring, at the third level trigger, a positron with an energy greater than 4 GeV at a position outside a radius of 25 cm on the calorimeter.

In order to select neutral current DIS events offline, the following cuts were applied, defining a fiducial sample:

- kinematic cuts: $Q^2_{\mathrm{DA}} > 120 \, \mathrm{GeV}^2$, $x_{\mathrm{DA}} > 10^{-3}$, $y_{\mathrm{JB}} > 0.05$;

- cuts to ensure the quality of the positron reconstruction:

  ○ The radial position of the positron track impact point on the rear calorimeter surface was required to exceed 36 cm;
  ○ $E_{\mathrm{DA}} > 10 \, \mathrm{GeV}$;
  ○ $E_{\mathrm{cne}} < 5 \, \mathrm{GeV}$, where E_{cne} is the energy, not associated with the positron, found inside a cone having an (η, ϕ)-radius $R = \sqrt{(\Delta\phi)^2 + (\Delta\eta)^2} = 0.8$ around the track of the positron candidate;

- suppression of photoproduction events:

  ○ $y_{\mathrm{el}} < 0.90$, where y_{el} is calculated from the scattered electron;
  ○ $35 \, \mathrm{GeV} < \sum_{\mathrm{EFOs}}(E - p_Z) < 65 \, \mathrm{GeV}$, where the sum runs over the energy- and Z-components of all EFO four-momenta;
  ○ DCA $< 10 \, \mathrm{cm}$, where DCA is the distance of closest approach of the positron track to the centre of the cluster of CAL cells assigned to it;

- vertex cut: Z position of the event vertex, $|Z_{\mathrm{VTX}}| < 50 \, \mathrm{cm}$, consistent with an ep interaction;

- restriction of the data sample to a region, where the QCDINS MC calculation is reliable: $Q'^2_{\mathrm{DA}} > 140 \, \mathrm{GeV}^2$.

Figure 2 shows the measured Q'^2_{DA} distribution, compared to various MC predictions. There is agreement between data and the standard DJANGOH DIS MC sample at a level of about 10 %. A larger discrepancy is seen between the data and the HERWIG MC sample. Also shown is the prediction of the QCDINS MC program, normalised to the number of events in the data. It has a very different distribution from both the data and the standard DIS events.

No cut was made on the variable x' for the standard DIS MC sample and the data because x' cannot be well reconstructed. On the other hand, the QCDINS Monte Carlo sample

includes a cut on the generated variable $x' > 0.35$. Lattice calculations show a steep decrease of the instanton contribution towards small values of $x' < 0.35$, corresponding to a small separation between instantons and anti-instantons, suggesting that this region can be neglected [35, 7, 15].

Application of the above cuts resulted in a sample of 91846 events for the data. Normalised to the data luminosity, QCDINS predicts 578 events, DJANGOH predicts 88300 and HERWIG predicts 76400 events. The corresponding predicted instanton cross section is 8.9 pb. The statistical uncertainties on these numbers are negligible compared to the uncertainty on the luminosity.

The discrepancy in the number of events predicted by HERWIG and DJANGOH can be traced to the cut in Q'^2, and arises from differences in the Q'^2 reconstruction due to the different hadronisation models in the MC programs. Without this cut, the numbers agree within the estimated uncertainty.

In the subsequent analysis, numbers of standard DIS Monte Carlo events were normalised to the number of data events in the fiducial sample, where the predicted QCDINS contribution is negligible ($\approx 0.7\%$).

6 Definition of discriminating variables

Two kinds of discriminating variables have been considered: those connected with the kinematics of an instanton-induced event and those connected with the final-state particles of the instanton system, the so-called shape variables. The kinematic variables chosen were Q'^2_{DA}, (see Fig. 1 and Section 3) and p_T^{jet}, the transverse momentum of the current jet in the hcms.

The shape variables were calculated from a subset of hadronic final state EFOs assigned to the instanton, referred to as the "instanton region" in what follows. The instanton region comprises all EFOs which were not assigned to the current jet and lay in the hemisphere opposite to the outgoing proton remnant, i.e. polar angle $\theta_{\text{EFO}}^{\text{hcms}} > 90°$. Once the instanton region was identified, the following shape variables were calculated:

- N_{EFO}, the multiplicity of EFOs;

- N_{EFT}, the multiplicity of tracks, that were used in constructing these EFOs;

- C, the circularity; this is a measure of the isotropy of EFOs in the hcms with respect to the photon-proton axis. To determine the circularity, the normalised two-dimensional momentum tensor,

$$M_{\alpha\beta}^{(2\text{D})} = \frac{\sum_j p_{j,\alpha} p_{j,\beta}}{\sum_j \left(p_{j,X}^2 + p_{j,Y}^2 \right)} \quad \text{with } \alpha, \beta = X, Y$$

6

was computed in the hcms from the three-momenta of the EFOs, requiring the number of EFOs to be larger than two. From its eigenvalues λ_1, λ_2, with $\lambda_1 > \lambda_2$, the circularity C was then obtained: $C = 2(1 - \lambda_1)$.

- S, the sphericity; this is a measure of how isotropically a collection of three-momenta is distributed. Large values correspond to a more isotropic distribution. The normalised momentum tensor, calculated from the EFOs in their centre-of-mass frame,

$$M_{\alpha\beta}^{(3D)} = \frac{\sum_j p_{j,\alpha} p_{j,\beta}}{\sum_j \left(p_{j,X}^2 + p_{j,Y}^2 + p_{j,Z}^2 \right)} \quad \text{with } \alpha, \beta = X, Y, Z \quad,$$

  has eigenvalues Q_1, Q_2, Q_3 with $0 \leq Q_1 \leq Q_2 \leq Q_3$. The sphericity is defined as $S = 3/2 \cdot (Q_1 + Q_2)$. The number of EFOs for this calculation had to be larger than two.

- ϵ', a measure of the density of the pseudorapidity η of EFOs in the hcms; to calculate ϵ', the EFOs were sorted with respect to the pseudorapidity η in the hcms, yielding N_{EFO} values $\eta_1, \eta_2, \ldots, \eta_{N_{\text{EFO}}}$. The closed interval $[\eta_i, \eta_{i+k}]$, $i+k \leq N_{\text{EFO}}$ thus contains $k + 1$ EFOs. The variable ϵ' is then defined by $\epsilon' = \epsilon_c - b(N_{\text{EFO}} - N_0)$ with $b = 0.339$, $N_0 = 30$ and

$$\epsilon_c = \frac{k}{N_{\text{EFO}} - k} \sum_{i=1}^{N_{\text{EFO}} - k} \frac{1}{\eta_{i+k} - \eta_i} \quad \text{where} \quad k = \left\{ \begin{array}{ll} N_{\text{EFO}}/2 & \text{for } N_{\text{EFO}} \text{ even,} \\ (N_{\text{EFO}} + 1)/2 & \text{for } N_{\text{EFO}} \text{ odd.} \end{array} \right.$$

  A more detailed description and justification of the numbers b and N_0 can be found elsewhere [36].

Figures 3 and 4 show the distributions of the discriminating variables in the fiducial sample (see Section 5). The contribution of instanton-induced events is 0.7 % according to the predictions of the QCDINS calculation. None of the variables have been corrected for detector or trigger effects.

In general, there is a qualitative agreement between the shape of the data and the DIS MC samples DJANGOH and HERWIG. The QCDINS predictions, normalised to the number of data events, show quite different distributions, indicating the suitability of these variables for separating instanton induced events from background.

However, the data are not reproduced in detail by the DIS MC simulations. Moreover, the two DIS MC descriptions differ from each other by a similar degree as from the data. For the DJANGOH sample, a parameter in the JETSET fragmentation program was tuned, as described in Section 4, so that the sphericity distribution of the data is reproduced, as shown in Fig. 4a. The description of the other variables, however, as shown in the figures, is not improved.

Given the uncertainties of the DIS MC predictions, and the smallness of the instanton contribution, it is not possible to make a reliable background subtraction.

7   Instanton enhancement

Several enhancement methods were compared to each other using the following criteria: From the numbers

$N_O(I_O)$:   number of standard DIS MC (QCDINS) events in the fiducial sample and

$N_E(I_E)$:   number of standard DIS MC (QCDINS) events in the instanton enhanced

sample,

the efficiencies r_I, of QCDINS and r_N, of the standard DIS MC samples were obtained according to $r_I = I_E/I_O$ and $r_N = N_E/N_O$. Values of the separation power, $P_s = r_I/r_N$, were then compared for different samples of similar QCDINS efficiency.

The enhancement methods investigated [36] comprised a combination of one-dimensional cuts on the discriminating variables, an optimised choice of two-dimensional cuts and the Fisher algorithm [37, 38], which performed best.

The Fisher algorithm was used to separate standard DIS and instanton events by cutting on a linear combination of the variables x_i. For n input variables x_i, $i = 1, 2, \ldots, n$, the mean values $\overline{x_i}^s$ for the signal and $\overline{x_i}^b$ for the background were determined. The correlation matrices between the variables were calculated according to

$$V_{ik,s} = \frac{1}{N} \sum_{\text{events}} (x_i^s - \overline{x_i}^s)(x_k^s - \overline{x_k}^s)$$

for the signal sample, and equivalently for the background ($V_{ik,b}$). These were averaged, $\overline{V}_{ik} = \frac{1}{2}(V_{ik,s} + V_{ik,b})$, and the resulting matrix was inverted. The Fisher discriminant is defined as

$$t = \sum_{i=1}^{n} w_i x_i \quad , \quad \text{with } w_i = \sum_{k} (\overline{V}^{-1})_{ik}(\overline{x_k}^s - \overline{x_k}^b) \quad .$$

Carli and Koblitz [39] have proposed a strategy to look for instanton-induced processes, using variables resulting from a careful optimisation procedure. An analysis with their variables, using the Fisher algorithm for signal enhancement, was also carried out. In addition, an analysis was carried out with a combination of their variables and those of Section 6. No significant improvement, as measured by the separation power P_s, was achieved.

8 Background-independent limits

In order to be independent of the standard DIS MC prediction, a conservative upper limit was set by assuming that all observed events after instanton-enhancement cuts are signal, i.e. the standard DIS background was zero.

To derive limits on the cross section, the QCDINS MC program was assumed to give a correct description of instanton-induced events. For signal enhancement the Fisher algorithm was used, with the QCDINS sample as signal and the DJANGOH sample as background. In this procedure, the DJANGOH background sample is only used to determine a good discriminating function; a non-optimal choice of background MC events will imply only that the instanton sensitivity of the measurement is not the highest achievable in principle.

The Fisher discriminant was calculated from all six discriminating variables described in Section 6 (S, C, $\log(p_T^{\text{jet}})$,N_{EFO}, N_{EFT}, ϵ'). In addition, a cut $Q'^2_{\text{DA}} < 250\,\text{GeV}^2$ was imposed, to improve instanton enhancement.

The distribution of the Fisher discriminant t for the data, the QCDINS signal sample and the DJANGOH background sample is shown in Fig. 5. The distributions for the DIS MC simulation and the data are rather similar, with the curve of the instanton signal being well separated. The distribution normalised to the predicted instanton fraction is also shown.

The numbers of data events above various values of the discriminating variable t are shown in Table 1. Also included are the numbers for the standard DIS MC samples. These are slightly larger than the number of data events. This is not surprising, since extremely restrictive cuts have been chosen, which only keep events in the tails of the standard DIS distributions. Problems are therefore expected in the modelling of the data.

The number of data events kept by each cut, N_d, was then compared with the theoretically predicted number of instanton events, N_{th}. The ratio N_d/N_{th} is equal to the ratio of cross-sections $R = \sigma_d/\sigma_{\text{th}}$, where $\sigma_{\text{th}} = 8.9\,\text{pb}$ is the theoretically predicted instanton cross section for the cuts of the fiducial sample, and σ_d is the instanton cross section computed for the same cuts, assuming that all data events are signal. This is true under the assumption that, with zero background, the acceptances of the observed events and of the QCDINS MC sample are equal. Figure 6 shows the ratio $R = \sigma_d/\sigma_{\text{th}}$, as a function of r_I, the fraction of instanton-induced events remaining in the sample after various cuts in the Fisher t variable.

In addition to the statistical uncertainties, uncertainties on the ratio R were taken into account by considering a $\pm 3\%$ change in the CAL energy scale, a change in the definition of the instanton region (see Section 6), and using Q^2 computed by the scattered electron

variables instead of $Q^2_{\rm DA}$.

Another uncertainty stems from the cuts made on the variables Q'^2 and x' by the QCDINS MC program at event generation, $x' > 0.35$ and $Q'^2 > 113\,{\rm GeV}^2$. These variables cannot be reconstructed well in the data. Therefore, the data might include some instanton-induced events with real x', Q'^2 values below these cut values. If, with the help of an accurate reconstruction of Q'^2 and x', these events could be removed from the data sample, it would lower the ratio R, yielding a value closer to the theoretical prediction.

From the value of R and its uncertainties, an upper limit for the instanton cross section can be derived for any given choice of r_I. For example, at $r_I = 10\%$, the upper limit would be 30 pb, to be compared with the theoretically predicted value of 8.9 pb. In a similar analysis by the H1 collaboration [8], in a region of phase space with a lower range of Q^2 ($10\,{\rm GeV}^2 < Q^2 < 100\,{\rm GeV}^2$), and at a comparable value $r_I = 10\%$, an upper limit of 221 pb at a 95 % confidence level (c.l.) was reported. This value is about a factor of five above the corresponding theoretical prediction.

In order to derive a conservative upper limit without an explicit choice of r_I, the t distribution was computed for a range of values of the instanton cross section. For a specific choice of the cross section, the t distributions for data and instanton events become equal at a certain specific value t_0, the instanton distribution overshooting the data for $t > t_0$. An upper limit can then be set by choosing the instanton cross section such that the number of instanton events exceeds the number of data events for $t > t_0$ at a (one sided) 95% c.l. This method yields an upper limit at a 95% c.l. for the instanton cross section, $\sigma_{\rm inst}$, of

$$\sigma_{\rm inst} < 26\,{\rm pb},$$

to be compared with the theoretically predicted cross section of 8.9 pb. The fraction of instanton-induced events remaining after the cut was $r_I = 4.6\%$.

9 Conclusion

A search for QCD-instanton-induced events has been performed in neutral current deep inelastic ep scattering, based on an integrated luminosity of $38\,{\rm pb}^{-1}$ in the kinematic range $Q^2 > 120\,{\rm GeV}^2$, $x > 10^{-3}$. Cuts on the Fisher discriminant have been used to obtain instanton-enhanced subsamples.

Assuming that all data events belong to an instanton signal, a conservative background-independent upper limit on the instanton cross section of 26 pb at a 95% c.l. has been set, to be compared to the theoretically predicted cross section of 8.9 pb.

10   Acknowledgements

References

[1] A. Belavin et al., Phys. Lett. **B 59**, 85 (1975).

[2] G. 't Hooft, Phys. Rev. Lett. **37**, 8 (1976);
G. 't Hooft, Phys. Rev. **D 14**, 3432 (1976). Erratum in Phys. Rev. D18, 2199 (1978);
G. 't Hooft, Phys. Rep. **142**, 357 (1986).

[3] H. Aoyama and H. Goldberg, Phys. Lett. **B 188**, 506 (1987);
A. Ringwald, Nucl. Phys. **B 330**, 1 (1990);
O. Espinosa, Nucl. Phys. **B 343**, 310 (1990);
A. Ringwald et al., Nucl. Phys. **B 365**, 3 (1991);
M. Gibbs et al., Z. Phys. **C 66**, 285 (1995);
A. Ringwald, Phys. Lett. **B 555**, 227 (2002).

[4] A. Ringwald and F. Schrempp, *Proc. 8th Int. Seminar, Vladimir,Russia, 1994*,
D. Grigoriev et al. (ed.), p. 170. World Scientific, Singapore (1995).

[5] I. Balitsky and V. Braun, Phys. Lett. **B 314**, 237 (1993).

[6] S. Moch et al., Nucl. Phys. **B 507**, 134 (1997).

[7] A. Ringwald and F. Schrempp, Phys. Lett. **B 459**, 249 (1999).

[8] H1 Coll., C. Adloff et al., Eur. Phys. J. **C 25**, 495 (2002).

[9] ZEUS Coll., U. Holm (ed.), *The ZEUS Detector*. Status Report (unpublished),
DESY (1993), available on `http://www-zeus.desy.de/bluebook/bluebook.html`.

[10] N. Harnew et al., Nucl. Inst. Meth. **A 279**, 290 (1989);
B. Foster et al., Nucl. Phys. Proc. Suppl. **B 32**, 181 (1993);
B. Foster et al., Nucl. Inst. Meth. **A 338**, 254 (1994).

[11] M. Derrick et al., Nucl. Inst. Meth. **A 309**, 77 (1991);
A. Andresen et al., Nucl. Inst. Meth. **A 309**, 101 (1991);
A. Caldwell et al., Nucl. Inst. Meth. **A 321**, 356 (1992);
A. Bernstein et al., Nucl. Inst. Meth. **A 336**, 23 (1993).

[12] J. Andruszków et al., Preprint DESY-92-066, DESY, 1992.

[13] A. Ringwald and F. Schrempp, Phys. Lett. **B 438**, 217 (1998).

[14] A. Ringwald and F. Schrempp, Comp. Phys. Comm. **132**, 267 (2000).

[15] A. Ringwald and F. Schrempp, Phys. Rev. Lett. **B 503**, 331 (2001);
M. Gibbs, A. Ringwald and F. Schrempp, *Proc.Workshop on Deep Inelastic Scattering and QCD (DIS95)*, J.-F. Laporte and Y. Sirois (eds.), p. 341. Ecole Polytechnique, Paris (1995).

[16] G. Marchesini and B.R. Webber, Nucl. Phys. **B 310**, 461 (1988);
G. Marchesini et al., Comp. Phys. Comm. **67**, 465 (1992).

[17] R. Brun, Preprint CERN-DD/EE 84-1, (1987).

[18] G. Ingelman, A. Edin and J. Rathsman, Comp. Phys. Comm. **101**, 108 (1997).

[19] A. Kwiatkowski, H. Spiesberger and H.-J. Möhring, Comp. Phys. Comm.
69, 155 (1992). Also in *Proc. Workshop Physics at HERA*, 1991, DESY, Hamburg.

[20] K. Charchula, G.A. Schuler and H. Spiesberger, Comp. Phys. Comm.
81, 381 (1994).

[21] H.L. Lai et al., Phys. Rev. **D 55**, 1280 (1997).

[22] G. Gustafson and U. Pettersson, Nucl. Phys. **B 306**, 746 (1988);
G. Gustafson, Phys. Lett. **B 175**, 453 (1986);
B. Andersson et al., Z. Phys. **C 43**, 625 (1989).

[23] L. Lönnblad, Comp. Phys. Comm. **71**, 15 (1992).

[24] B. Andersson et al., Phys. Rep. **97**, 31 (1983).

[25] T. Sjöstrand, Comp. Phys. Comm. **82**, 74 (1994);
T. Sjöstrand, Preprint CERN-TH.7112/93,LU TP 95-20, 1993.

[26] ZEUS Coll., J. Breitweg et al., Phys. Lett. **B 421**, 368 (1998).

[27] B. R. Webber, Nucl. Phys. **B 238**, 492 (1984).

[28] G.M. Briskin. Ph.D. Thesis, Tel Aviv University, 1998;
ZEUS Coll., J. Breitweg et al., Eur. Phys. J. **C 1**, 81 (1998).

[29] H. Abramowicz, A. Caldwell and R. Sinkus, Nucl. Inst. Meth. **A 365**, 508 (1995);
R. Sinkus and T. Voss, Nucl. Inst. Meth. **A 391**, 360 (1997).

[30] S. Bentvelsen, J. Engelen and P. Kooijman, *Proc. Workshop on Physics at HERA*,
W. Buchmüller and G. Ingelman (eds.), Vol. 1, p. 23. Hamburg, Germany, DESY
(1992);
K.C. Höger, *Proc. Workshop on Physics at HERA*, W. Buchmüller and
G. Ingelman (eds.), Vol. 1, p. 43. Hamburg, Germany, DESY (1992).

[31] F. Jacquet and A. Blondel, *Proceedings of the Study for an ep Facility for Europe*,
U. Amaldi (ed.), p. 391. Hamburg, Germany (1979). Also in preprint DESY 79/48.

[32] S.Catani et al., Nucl. Phys. **B406**, 187 (1993).

[33] S.D. Ellis and D.E. Soper, Phys. Rev. **D 48**, 3160 (1993).

[34] W. H. Smith, K.Tokushuku and L.Wiggers, *Proc. Computing in High-Energy
Physics (CHEP)*, C. Verkerk and W. Wojcik (eds.), p. 222. CERN (1992).

[35] A. Ringwald and F. Schrempp, *Proc. 8th.Int.Workshop on Deep-Inelastic Scattering, Liverpool (DIS2000)*, J. A. Gracey and T. Greenshaw (eds.), p. 318. World Scientific, Singapore (2001). Also in preprint hep-ph/0006215, (2000).

[36] S. Hillert. Ph.D. Thesis, Universität Hamburg, 2002, available on `http://www-library.desy.de/preparch/desy/thesis/desy-thesis-02-052.ps.gz`.

[37] R. A. Fisher, Ann. Eug. **7**, 179 (1936).

[38] V. Blobel and E. Lohrmann, *Statistische und numerische Methoden der Datenanalyse.* Teubner, Stuttgart, Leipzig, (1998).

[39] T.Carli and B.Koblitz, Preprint hep-ph/0011224, (2000).

	r_I [%]	DATA	QCDINS	DJANGOH	P_S	HERWIG	P_S
$t > 8.0$	32.6	1847 ± 43	188.5 ± 1.7	2592 ± 26	12	2145 ± 27	14
$t > 8.5$	24.0	925 ± 30	139.0 ± 1.4	1338 ± 19	17	1091 ± 19	21
$t > 9.0$	16.4	424 ± 21	95.1 ± 1.2	630.2 ± 13	24	524.1 ± 13	29
$t > 9.5$	10.1	179 ± 13	58.4 ± 0.9	263.8 ± 8.3	36	229.5 ± 8.8	41
$t > 10.0$	5.5	76 ± 8.7	31.8 ± 0.7	105.6 ± 5.3	49	89.8 ± 5.5	58
$t > 10.5$	2.7	33 ± 5.7	15.7 ± 0.5	35.1 ± 3.0	73	35.1 ± 3.4	73

Table 1: *Numbers of events within instanton enhancing cuts chosen such that a fraction r_I of the QCDINS sample within fiducial cuts (see Sect. 5.2) is kept. Statistical errors are given. The separation power P_S is also shown (see Sect. 7).*
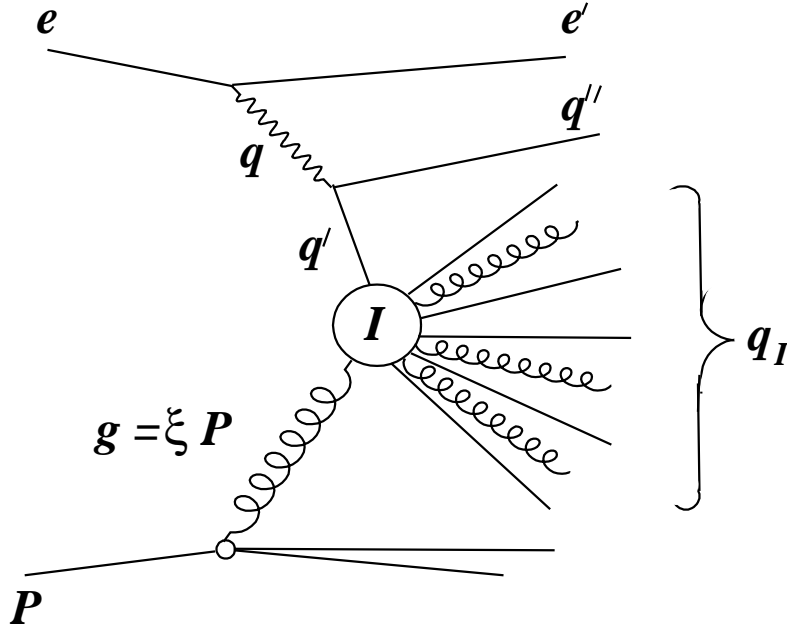
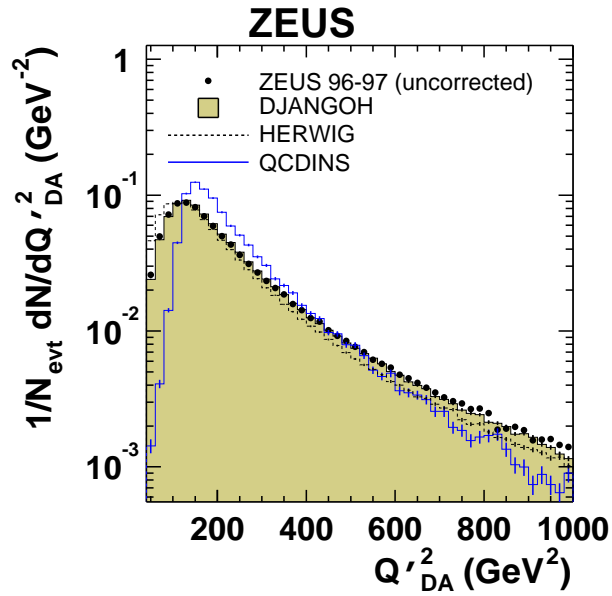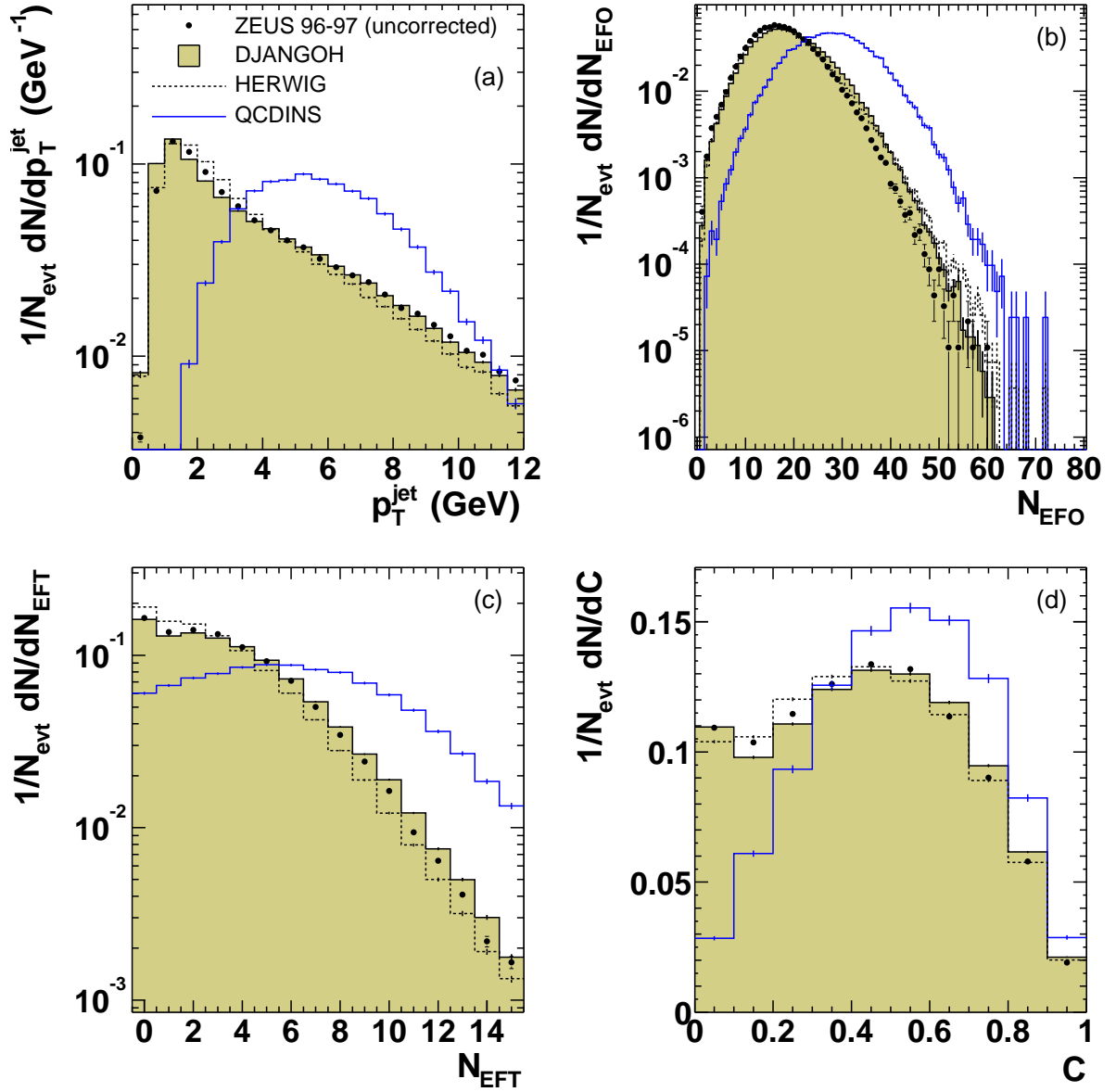**Figure 1:** *Kinematics of instanton-induced ep collisions.*

Figure 2: *Distribution of the kinematic variable Q'^2_{DA} describing the hard subprocess of instanton-induced events. Statistical error bars are given.*

ZEUS

Figure 3: *Distributions of variables calculated from the instanton region, shown for the fiducial sample: (a) the transverse momentum, p_T^{jet}, of the current jet, (b) EFO multiplicity, N_{EFO}, (c) EFO track multiplicity, N_{EFT}, (d) circularity, C, in the hcms. Statistical errors are given.*
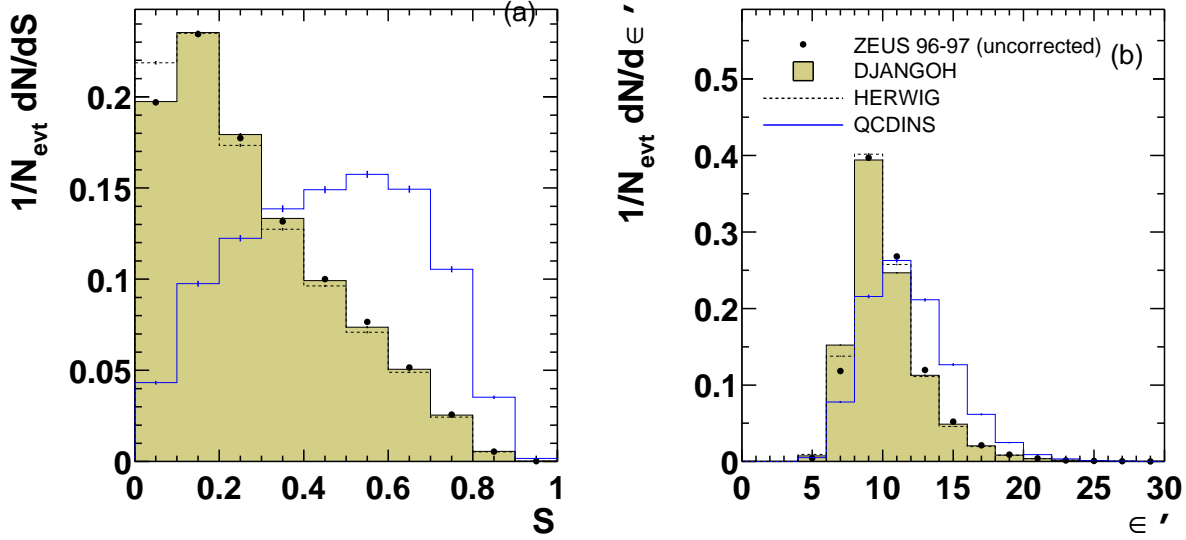
ZEUS

Figure 4: *Distributions of two of the shape variables for the fiducial sample (a) sphericity S, (b) ϵ'.*
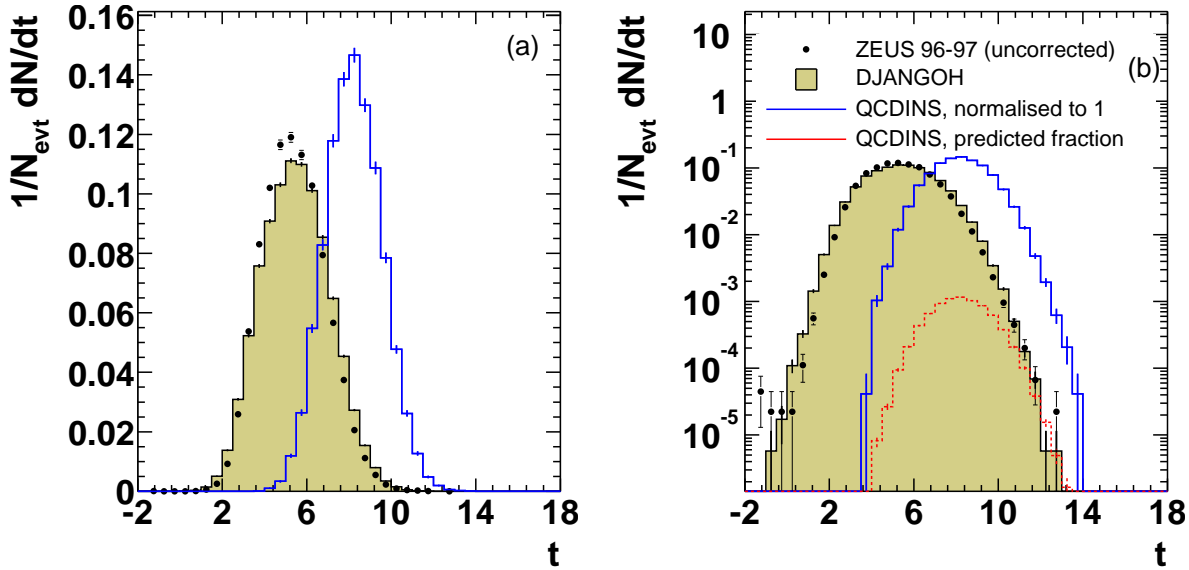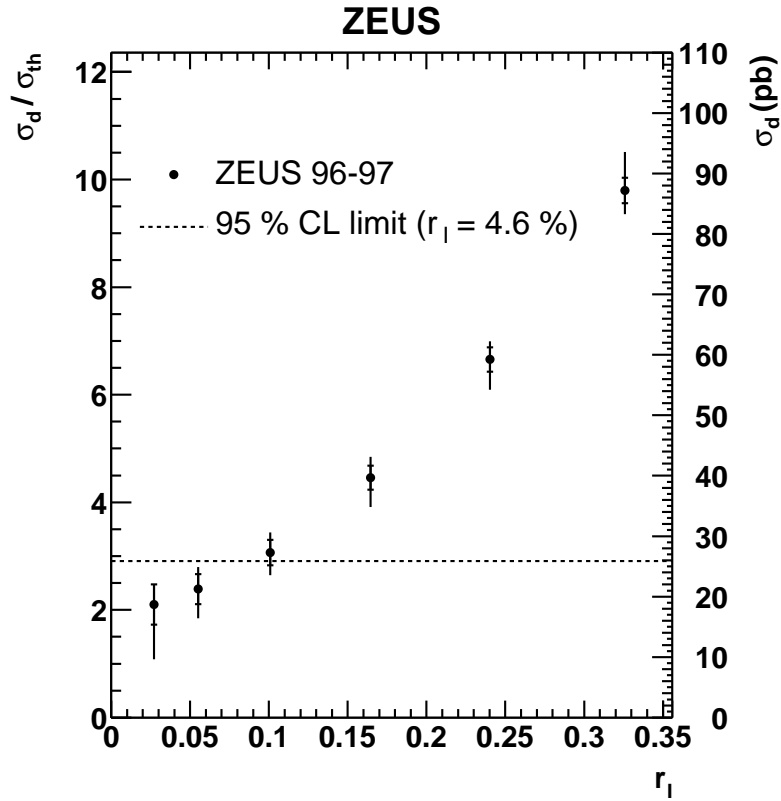
ZEUS

Figure 5: *Fisher discriminant t calculated from the variables S, C, p_T^{jet}, N_{EFO}, N_{EFT} and ϵ'. Shown are (a) linear and (b) logarithmic plots for the fiducial sample with an additional cut $Q_{\text{DA}}'^2 < 250\,\text{GeV}^2$. In (b), the QCDINS distribution, normalised to the predicted fraction of 0.79%, is also shown.*

Figure 6: *Plot of the ratio of the cross sections $\sigma_d/\sigma_{\mathrm{th}}$ vs. r_I, the fraction of instanton-induced events remaining after the specific cut in t. The cross sections σ_d and σ_{th} refer to the measured cross-section and to the cross-section of instanton-induced events according to the QCDINS Monte Carlo generator, respectively. Inner error bars correspond to statistical errors, outer error bars show statistical and systematic errors added in quadrature. The scale on the right hand side gives the measured cross section in the kinematic region of the fiducial sample. The dashed line is a conservative 95% c.l. (see text), corresponding to $r_I = 4.6\%$.*